RSC Advances

PAPER

View Article Online
View Journal | View Issue

Cite this: *RSC Adv.*, 2018, **8**, 19906

Improving the anti-icing/frosting property of a nanostructured superhydrophobic surface by the optimum selection of a surface modifier†

Zhiping Zuo, *[ab] Ruijin Liao,[b] Xiaoyu Song,[c] Xuetong Zhao[b] and Yuan Yuan[d]

To understand the effect of chemical composition on the anti-icing properties of a nanostructured superhydrophobic surface (SHP), four SHP surfaces were prepared on glass, which was initially roughed by a radio frequency (RF) magnetron sputtering method and then modified with HDTMS (a siloxane coupling agent), G502 (a partially fluorinated siloxane coupling agent), FAS-17 (a fully fluorinated siloxane coupling agent) and PDMS (a kind of polysilicone widely used in power transmission lines). Results show that the anti-icing properties of these four SHP surfaces in glaze ice varied wildly and the as-prepared SHP surface which was modified with FAS-17 (SHP-FAS) demonstrated a superior anti-icing/frosting performance. Approximately 56% of the entire SHP-FAS remained free of ice after spraying it for 60 min with glaze ice, and the average delay-frosting time (the time taken for the whole surface to become covered with frost) was more than 320 min at −5 °C. Equivalent model analysis indicates that ΔG, defined as the difference in free energy of the Cassie–Baxter and Wenzel states, of the SHP-FAS is much lower than the other three SHP surfaces, giving priority to Cassie state condensation and the self-transfer phenomenon helping to effectively inhibit the frosting process by delaying the ice-bridging process, which is beneficial for improving the anti-frosting property. This work sheds light on and improves understanding of the relationship between anti-icing and anti-frosting properties and is helpful in making the optimum selection of a surface modifier for improving the anti-frosting/icing performances of a SHP surface.

Received 23rd January 2018
Accepted 14th May 2018

DOI: 10.1039/c8ra00712h

rsc.li/rsc-advances

1. Introduction

Ice accumulation adversely affects numerous commercial sectors including aircrafts, telecommunications, automotives, wind turbines and power lines.[1] A glass insulator is one of the most important components in a transmission line and the icing of an insulator surface may lead to serious consequences, such as flashover incidents, collapsing of towers and power failures.[2,3] Traditional anti-icing methods including AC-hot de-icing methods and manual de-icing methods include problems with time consumption and low efficiency. Meanwhile, the irregular shape of insulators hinders the development of automatic de-icing devices. Therefore, measures to inhibit the accumulation of ice on surfaces which are exposed to cold regions are urgently needed. Inspired by the "lotus effect",[4,5] superhydrophobic (SHP) surfaces are believed to be potential candidates for achieving anti-icing properties because of their excellent water repelling abilities. Considerable interest has been generated for utilizing SHP surfaces for anti-icing applications.[6]

The SHP surface has been proven to be helpful in improving anti-icing properties by delaying ice formation,[7] enhancing the dynamic anti-icing behavior of water droplets impacting the SHP surface,[8] reducing the ice adhesion strength,[9] and so forth. Slippery liquid-infused porous surfaces (SLIPS) also demonstrate an excellent ice adhesion force. But the SLIPS may not be suitable for application on transmission lines because of the high voltage.[10–13] Huang *et al.* prepared a SHP surface by mixing silica sol and fluorinated acrylate copolymers and found that ice formation was delayed by 90 min at −5.6 °C.[14] Ruan *et al.*

[a]*School of Automation, Chongqing University, Chongqing 400044, China. E-mail: zpzuo@cqu.edu.cn*

[b]*State Key Laboratory of Power Transmission Equipment & System Security and New Technology, Chongqing University, Chongqing 400044, China*

[c]*Department of Electrical Engineering and Computer Science, College of Engineering & Applied Science, University of Cincinnati, Cincinnati, Ohio, 45221, USA*

[d]*College of Materials Science and Engineering, Chongqing University, Chongqing 400044, China*

† Electronic supplementary information (ESI) available: This supplementary information document contains the layout of the Peltier-based platform; an XRD pattern of the as-prepared surface before and after annealing treatment; CAs, SAs and the frosting process of bare glass after modification and a ZnO surface without modification; geometries of modifiers; chemical composition; schematic of the artificial climate chamber; freezing morphology of glass modified with FAS-17 and SHP-FAS in glaze ice; frost propagation; diagram of conversion of the ZnO nanostructures into cylindrical structures; surface roughness, CAs and SAs of the as-prepared four SHP samples; the self-transfer phenomenon on the FAS-modified SHP surface at −5 °C. See DOI: 10.1039/c8ra00712h

studied the anti-icing properties of SHP aluminum surfaces and found that the freezing temperature of static water droplets was lowered from −2.2 °C down to −6.1 °C.[15] Meanwhile some other researchers doubt the practical application of SHP surfaces in anti-icing applications.[16,17] They claim that frost formation could significantly compromise the icephobic properties of SHP surfaces, and frost nucleation could occur on all areas of the SHP surface leading to a loss of superhydrophobicity at low temperatures and high humidity.[18] The difference in the micro/nanostructures is believed to be the main reason for the above results. Recently, sporadic reports have shown that SHP nanostructures or hierarchical structures can effectively retard frosting.[19–21] Wen *et al.* designed a composite micro/nanostructured surface by using poly(vinylidene difluoride) (PVDF) polymer in combination with ZnO materials *via* heat-pattern-transfer and crystal-growth techniques, which displayed excellent anti-fogging and icing-delay properties.[22] Guo *et al.* investigated the dependence of the anti-frosting properties on the nano–micro/structure surface. A long frosting delay could be achieved for more than 185 min on the nanohair surface with a ratchet period of 290 μm under a temperature of −10 °C.[23] Hence, providing a SHP surface with optimum nanoscale textures is essential for improving the anti-icing properties. The general process for fabricating SHP surfaces involves two steps: construction of the micro/nanostructures and modification with low-surface-energy materials.[24,25] Apart from the textures, we believe that the surface modification, as one of the main fabrication steps, also has a large effect on the anti-icing properties of the SHP surfaces especially on the same desired nano-scale structures.[26–29] Commonly used surface modifiers mainly include long-chain alkanes, partially or fully fluorinated silanes and polydimethylsiloxane. Although considerable work has been conducted on modifying the structures in order to enhance the anti-frosting/icing properties of the SHP surfaces, a systematic investigation on the effect of chemical composition, endowed by various surface modifiers, on the frosting/freezing process has rarely been incorporated.

Another key factor, apart from intrinsic parameters such as textures and chemical compositions, leading to a differentiation in the anti-icing properties is the variation in experimental methods. The experimental methods commonly used to characterize anti-icing properties of SHP surfaces include water droplet impact dynamics, delay-icing time of water droplets, the freezing temperature of water droplets or anti-fogging properties *et al.* However, these experimental conditions are far from real freezing weather conditions with regards to water droplet size, ambient temperatures, rainfall, relative humidity and so forth. The same roughness which prevents the accumulation of ice under certain conditions can be detrimental in other environments.[30] A single nanostructure SHP surface showed a robust anti-icing performance owing to supercooled microdroplets partly rebounding off its surface in a wind tunnel.[31] Therefore, the accurate evaluation of anti-icing properties should be based on a reference environment.[31] Both field and laboratory investigations show that glaze ice is the most dangerous type of ice, associated with the highest probability of flashover in transmission lines.[32,33] However, studies on the anti-icing properties of SHP surfaces with various surface modifiers in glaze ice are still sorely lacking, and these are vital for the design of anti-icing coatings which can be applied to transmission lines. Besides, the SHP surfaces are exposed to an environment of low temperature and high humidity. Vapor condensation or the frosting process will inevitably occur during the freezing process of glaze ice. Investigations on the anti-frosting properties of a SHP surface is necessary in order to shed light on the anti-icing performance in glaze ice.

As stated in our previous work, microstructure defects on SHP surfaces would cause an adverse effect on the anti-icing performance in glaze ice as the continually impacting supercooled micro-scale water droplets rapidly accumulate on these defects leading to a dramatic increase in the freezing area.[34,35] Therefore, to accurately evaluate the effect of surface modification on the anti-icing property, the as-prepared SHP surfaces should be carefully prepared to minimize defects. Compared to other methods, a radio frequency (RF) magnetron sputtering method represents one of the simplest and most effective methods for easily developing proper nano-scale structures.[36–38] A SHP ZnO surface modified with HDTMS was prepared by an RF magnetron sputtering method as reported in our previous work, and exhibits excellent anti-icing performance.[39] The focus of the present work is to further improve the anti-icing properties of a ZnO SHP surface by selecting an optimum surface modifier. The excellent process stability of RF magnetron sputtering is beneficial for obtaining uniform nano-scale textures and for decreasing the number of defects as much as possible, which is helpful to accurately evaluate the effect of surface modifiers on the anti-icing properties.

In this study, an RF magnetron sputtering method was used to fabricate ZnO nanostructures, and four typical surface modifiers were used to modify the ZnO nanostructure to obtain superhydrophobicity. The surface morphology, chemical composition and wettability were investigated by corresponding methods. An artificial climate chamber was used to evaluate the effect of surface modifiers on the anti-icing properties of the nanostructured SHP surfaces in glaze ice. Furthermore, macroscopic and microscopic frosting processes of the four SHP surfaces were studied on a Peltier-based platform.

2. Experiments

2.1 Sample preparation

The glass slides were rinsed in deionized water, ultrasonically cleaned in ethanol, and dried prior to being used as substrates. The films were prepared by means of RF magnetron sputtering of a Zn target (Hezong XinCai Company, diameter, 61.5 mm; thickness, 5 mm). The vacuum chamber was pumped down to a base pressure of 4.0×10^{-3} Pa. Sputtering was carried out in Ar (99.99% purity) plasma under a working pressure of 1.5 Pa. The sputtering power was maintained at 100 W with a fixed target-substrate distance of 10 cm. Then the substrate was annealed in a muffle furnace under a normal ambient atmosphere from room temperature to 400 °C at a rate of 10 °C min^{-1}, maintained at 400 °C for 30 min and subsequently cooled down naturally to room temperature before undergoing

surface modification. Generally, different coupling agents with a low surface energy were used to lower the surface energy. As for hexadecyltrimethoxy silane ($CH_3(CH_2)_{15}Si(OCH_3)_3$, HDTMS, Aladdin Co., Ltd) and 1*H*,1*H*,2*H*,2*H*-perfluorodecyltrimethoxysilane ($CF_3(CF_2)_7CH_2CH_2Si(OCH_3)_3$, FAS-17, Aladdin Co., Ltd) molecules, the annealed substrates were immersed in an ethanol solution of 2 wt% HDTMS and 2 wt% FAS-17 for 30 min and subsequently dried at 90 °C for 30 min, respectively. Chemical vapor deposition was used to coat the polydimethylsiloxane (PDMS Sylgard 184, Dow Corning Co., Ltd) and dodecafluoroheptylpropyltrimethoxy silane ($C_{14}F_{12}H_{20}SiO_3$, G502, Harbin Xuejia Fluorin Silicon Chemical Co., Ltd) onto the annealed samples. 1.2 g PDMS or G502, and the annealed samples, were placed in a sealed jar and placed horizontally with a volume of 250 mL, and subsequently heat treated at 150 °C for 2 h. For the sake of description, the above four SHP surfaces were marked as SHP-HDTMS, SHP-FAS, SHP-PDMS and SHP-G502, respectively. For comparison, we also prepared glass surfaces modified with FAS-17, HDTMS, PDMS and G502.

2.2 Sample characterization

Surface morphology was studied by field emission scanning electron microscopy (FE-SEM, Nova 400, Japan). EDS was performed by SEM (Hitchi, SU8010, Japan). The surface roughness and chemical composition were analyzed by a probe-type surface profiler (Dektak 150, America) and X-ray photoelectron spectrometer (XPS, Thermo escalab 250Xi, America). The X-ray-photoelectron spectrometer was equipped with a monochromatic Al Kα X-ray source ($h\nu$ = 1486.6 eV). Survey spectra were taken from 0 to 1349 eV with a pass energy of 100 eV (source gun = mono 650 μm). The wettability of the sample was measured by a contact angle meter (Drop meter A-100, China). Five different spots for one sample were measured each time and the average value was regarded as the CA. The water volume was 10 μL. An artificial climate chamber was used to simulate glaze ice to evaluate the anti-icing property. The anti-frosting behaviors of the samples were investigated on a self-made Peltier-based platform. The system included a water-cooled circulating machine, a semiconductor refrigerating platform, peristaltic pump, a camera image acquisition system and a personal computer as shown in Fig. S1.†

3. Results and discussion

3.1 Surface morphology and wettability

Fig. 1 shows the SEM images of the samples before and after surface modification. After an annealing treatment at 400 °C, the Zn layer was transformed into ZnO with a hexagonal crystal phase (shown in Fig. S2†). The as-prepared ZnO SHP surfaces exhibited evident surface roughness with ZnO nanostructures randomly distributed on the whole surface. As shown in Fig. 1b with a higher magnification, the diameters of these nanostructures ranged from 42.1 nm to 135.1 nm. As shown in the SEM images of SHP-HDTMS, SHP-FAS, SHP-PDMS and SHP-G502, there is no apparent change of surface morphology observed after surface modification. Although some organic thin film may appear on the surfaces, the surface morphology remains relatively consistent, which is further confirmed by the measured surface roughness results of shown in the ESI, Table S1.† The roughness average (R_a) and the root-mean-square roughness (R_q) of the four SHP surfaces are almost consistent and within a range of 470 ± 5% nm and 565.4 ± 8% nm. Therefore, we can reasonably consider that the four SHP surfaces possess the same surface morphology.

As shown in Fig. S3,† the contact angles (CAs) of the glass surfaces modified with PDMS, G502, HDTMS, and FAS-17 are in the range of 93.7° to 108.9° demonstrating their hydrophobicity.[40] Water droplets easily adhered onto the glass surfaces modified with PDMS, G502, and HDTMS leading to sliding angles (SAs) larger than 66.8°. The SAs of glass surface modified with FAS-17 are lower than 20°. The as-prepared unmodified ZnO surface indicates a completely superhydrophilic property with water droplets almost completely drilling into the textures. Fig. 2 shows the CAs and SAs of the four as-prepared SHP surfaces. All of the surfaces exhibit superhydrophobicity with CAs larger than 160° and SAs smaller than 10° as shown in Table S2.† Water droplets can easily roll off the four SHP surfaces.

3.2 Chemical composition

Both EDS and XPS were used to analyze the chemical composition of the as-prepared samples before and after surface modification. The geometries of the FAS-17, G502, HDTMS, and PDMS ($n = 10$) molecules are illustrated in Fig. S4.† As shown in Fig. S5,† the EDS spectrum of the ZnO nanostructures prior to surface modification shows no other peaks apart from those of Zn and O, indicating the existence of ZnO. After modification with FAS-17 or G502, C, Si and F elements were detected in the EDS spectrum and a significant F(1s) peak appeared at 689.0 eV in the XPS spectrum, proving the existence of FAS-17 or G502 molecules.[41] Both EDS and XPS spectra reveal the presence of C after modification with HDTMS and PDMS molecules indicating that the HDTMS and PDMS molecules had successfully attached onto the ZnO nanostructures. These results confirm the successful attachment of low-surface-energy molecules to the ZnO surface after surface modification.

3.3 Anti-icing performance in glaze ice

To further investigate the effect of the surface modifiers on the anti-icing performance of the four SHP samples, an artificial climate chamber was used to simulate freezing weather. "Glaze ice" represents one of the most serious freezing conditions and thus was simulated to test the anti-icing performance of the four SHP surfaces.[32] A schematic of the artificial climate chamber is shown in Fig. S6† and the experimental conditions are set according to Table 1.

Though the SA of the glass surface modified with FAS-17 is lower than 20°, micro-scale water droplets can easily adhere onto the surface leading to poorer anti-icing properties compared to those for SHP-FAS, which indicates that nano-scale roughness is essential for enhancing the anti-icing performance in glaze ice, as shown in Fig. S7.† To shed light on the effect of

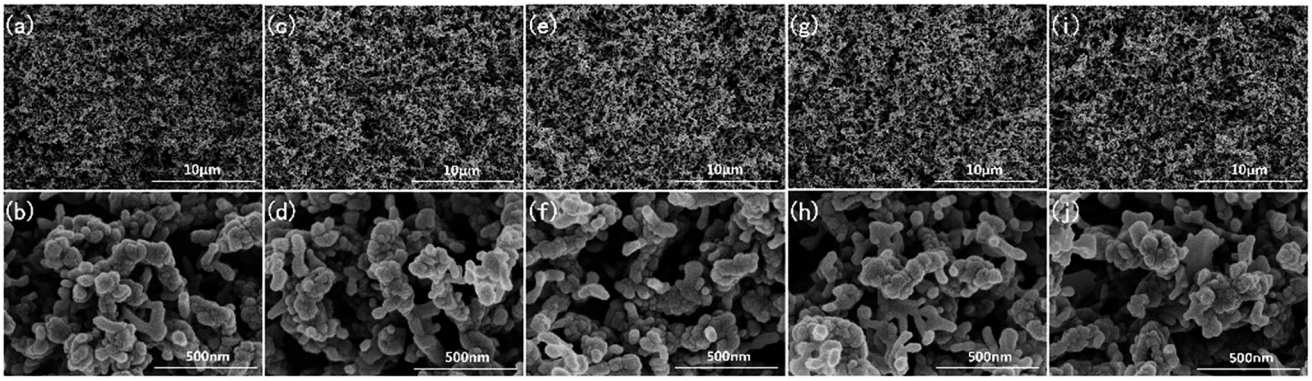

Fig. 1 SEM images of the ZnO nanostructures before (a and b) and after modification with FAS-17 (c and d), HDTMS (e and f), G502 (g and h), and PDMS (i and j).

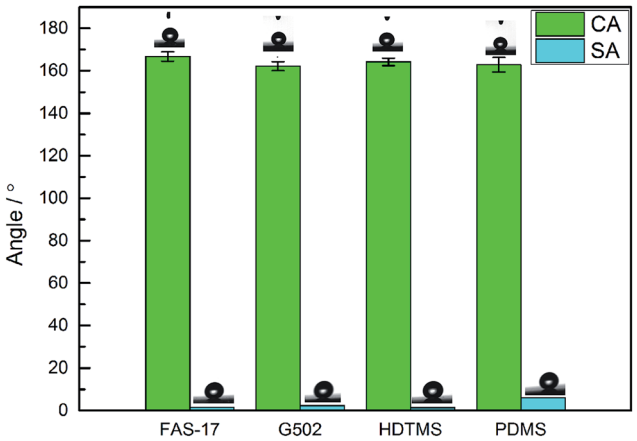

Fig. 2 CAs and SAs of the four as-prepared SHP surfaces.

surface modifiers on the anti-icing performance of nanostructured SHP surfaces, the four as-prepared SHP surfaces were placed in the artificial climate chamber. Fig. 3 and 4 show the freezing process of the four SHP surfaces in glaze ice over a 60 min time period. The freezing areas in glaze ice are the average values of two groups of identical samples. Though the four SHP surfaces demonstrate excellent water repellency at ambient temperatures, their anti-icing properties in glaze ice vary greatly. Supercooled water droplets were found to easily adhere onto the SHP-PDMS and SHP-G502 surfaces, which soon became covered with isolated ice particles. Almost 90% of the SHP-PDMS and SHP-G502 surfaces had frozen within 30 min. The ice particles slowly grew into long column-like icicles after a prolonged spraying time. SHP-HDTMS shows a better anti-icing performance with 52.1% of the surface remaining unfrozen after 30 min which increased up to 78.4% after 60 min. SHP-FAS exhibits the best anti-icing performance. Only 44.3% of the SHP-FAS surface had frozen after 60 min which is half of that for the SHP-PDMS and SHP-G502 surfaces. Due to the hydrophilicity of the edges, when sprayed, the supercooled water droplets would firstly adhere onto the upper edges of the as-prepared SHP surfaces leading to the formation of icicles. It was found that the long icicle, as marked by a red rectangle in Fig. 4, which grew from the upper side was not in close contact with the SHP-FAS surface but was at a wedge angle indicating a real freezing area smaller than 44.3%.

Table 1 Experimental conditions for glaze ice

Ambient temperature (°C)	-8 ± 1
Water temperature (°C)	4 ± 1
Wind velocity (m s^{-1})	3
Water flow rate (L h^{-1})	90
Water conductivity (μs cm^{-1})	255

3.4 Anti-frosting performance

The vapor condensation/frosting process inevitably occurs during glaze ice formation because of the high humidity and low temperatures in the artificial climate chamber. The anti-frosting performances of the as-prepared samples were investigated on a Peltier-based platform. The sample temperature was set at −5 °C. As shown in Fig. S8,† the glass surfaces modified with PDMS, G502, HDTMS, and FAS-17 as well as the as-prepared unmodified ZnO surface by RF magnetron sputtering showed poor anti-frosting properties with entire surfaces frozen in less than 10 min. Due to the hydrophilicity of the as-prepared unmodified ZnO surface, frost grew much more densely compared to that on the bare glass surfaces which had undergone modification. The frosting morphologies of the samples at 60 min varied obviously, which is probably a result of the different surface modifiers.

However, the four as-prepared SHP surfaces demonstrated improved anti-frosting properties as shown in Fig. 5. It was found that SHP-PDMS exhibited the poorest anti-frosting performance with a delayed-frosting time (time for the entire surface to be covered with frost) of less than 45 min. Obvious condensed water droplets were found on SHP-G502, SHP-FAS and SHP-HDTMS whose surface colors changed from dark grey to white in 45 min. A large area of the SHP-G502 and SHP-FAS surfaces remained free of frost except for a small amount of frost accumulating at the edges which is not apparent from a micro-point of view. An evident frost layer formed on the SHP-HDTMS surface within 45 min and slowly covered the entire

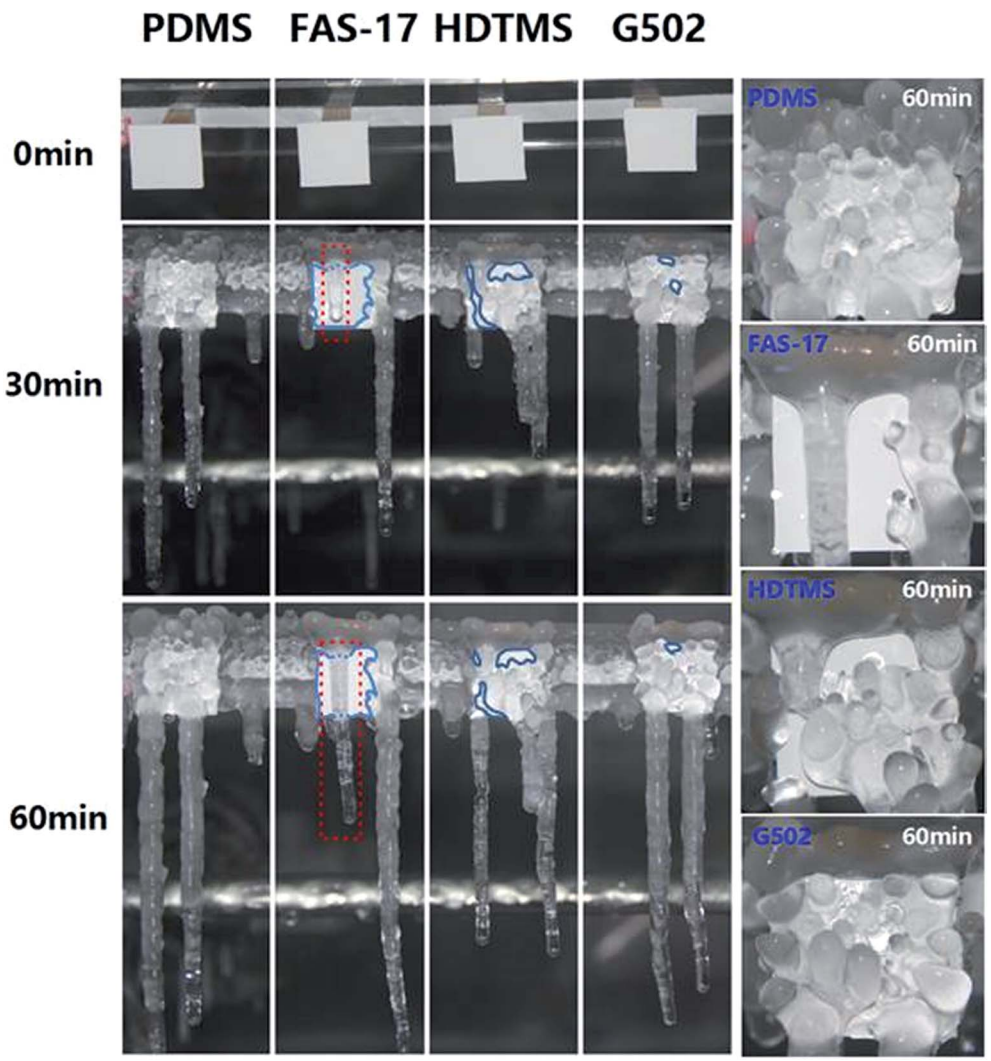

Fig. 3 Freezing morphology of the four as-prepared SHP surfaces.

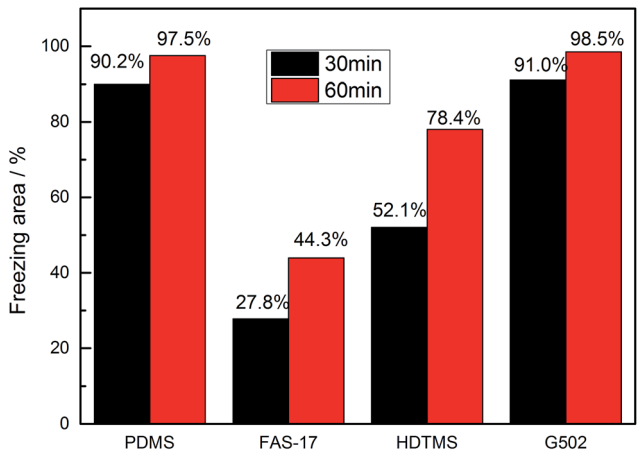

Fig. 4 Freezing areas of the four as-prepared SHP surfaces in glaze ice.

surface within 240 min. Interestingly, although frost on SHP-HDTMS appeared earlier than on SHP-G502, the frost propagated faster on the SHP-G502 surface leading to a 91% freezing area in 90 min. Compared to the other three SHP surfaces, SHP-FAS exhibited the best anti-frosting behavior. About 82% of the entire surface remained free of frost for 90 min and the frosting time was effectively delayed for about 320 min.

As the event of frosting may randomly occur on chilled solid surfaces, over 20 trials were conducted on the as-prepared SHP surfaces. Fig. 6 shows the frosting area of the four SHP surfaces as a function of freezing time. We can conclude that the SHP-PDMS surface displays the worst anti-frosting behavior with the whole surface freezing in less than 25 min. SHP-FAS demonstrates the best anti-frosting performance with an average frosting time delay of over 320 min, which is approximately 12.8 times that of SHP-PDMS. It is worth noting that the frost propagation on the four SHP surfaces slowly grew towards the unfrozen regions and no other clear defects were found during the whole experiment. Therefore, the difference in the experimental results can be ascribed to the effect of chemical

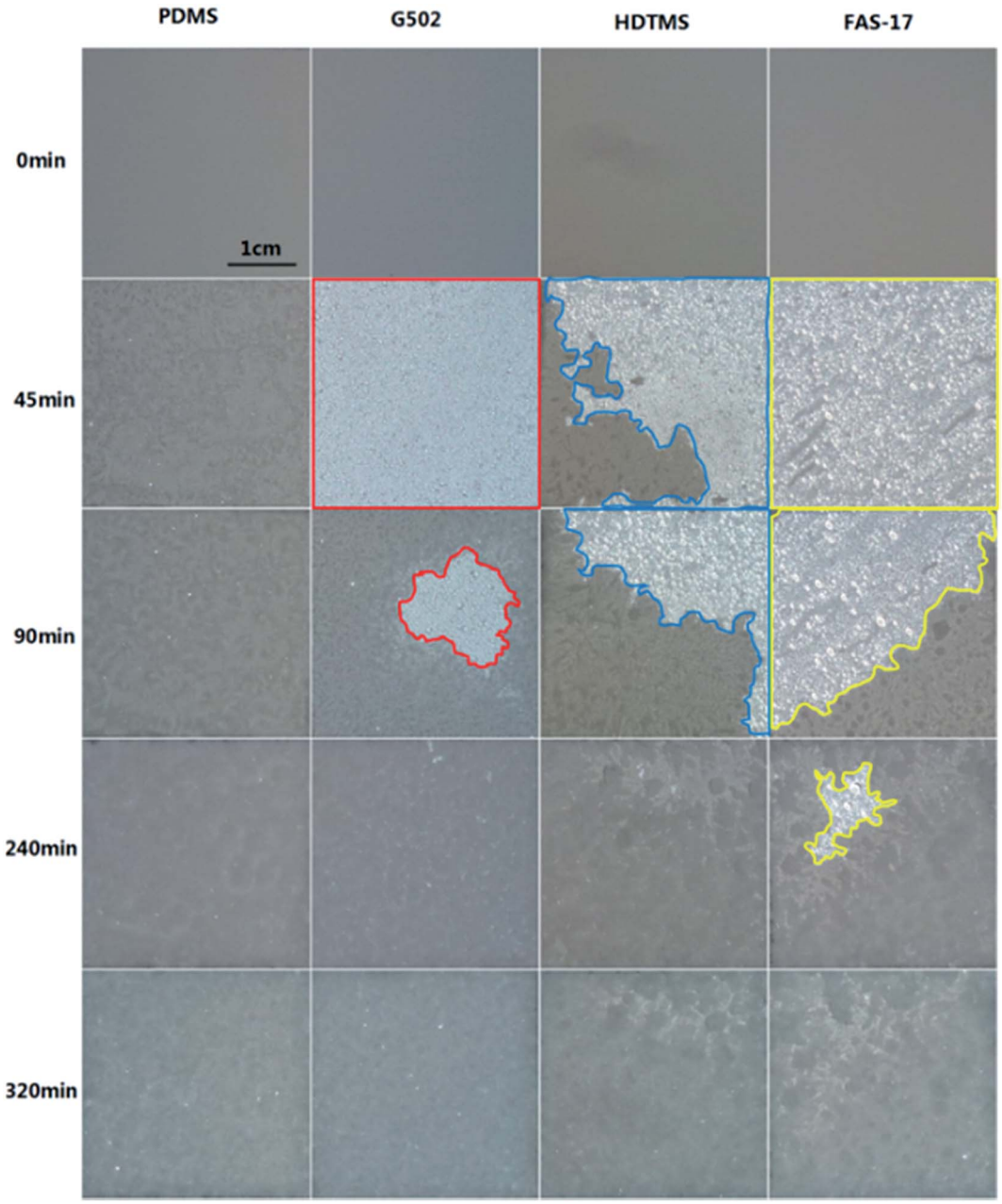

Fig. 5 The frosting process of ZnO surfaces modified by PDMS, G502, HDTMS and FAS-17.

composition ruling out the impact of structures. It can also be concluded that the anti-icing performances of the as-prepared SHP surfaces are closely related to their anti-frosting properties. The as-prepared SHP surfaces which demonstrate excellent anti-frosting properties are prone to having better anti-icing performances in glaze ice.

To clarify frost propagation on the four SHP surfaces, the microprocess of frosting on the four SHP surfaces was observed. Pictures captured at 10, 20, 30 and 40 min are displayed in Fig. 7. Obvious condensed microdroplets formed on the four SHP surfaces in 10 min. The condensed water droplets on the SHP-PDMS surface soon froze within 10 min, while the droplet size kept growing on the other three SHP surfaces. It is obvious that the growth pattern of the condensed water droplets on the other three SHP surfaces is quite different. The condensate droplets on the SHP-G502 surface grew larger mainly by merging with nearby condensed water and then remained almost motionless, resulting in comparatively homogeneous droplets. On the contrary, distribution of condensed water droplets on the SHP-HDTMS and SHP-FAS surfaces varied with time and the water volume was much smaller than that on the SHP-G502 surface, indicating a fairly dynamic property of condensed water droplets on SHP-HDTMS and SHP-FAS.

The dynamic process of condensed water droplets is shown in Fig. 8. With a prolonged freezing time, condensed microdroplets grew larger *via* vapor condensation and by the

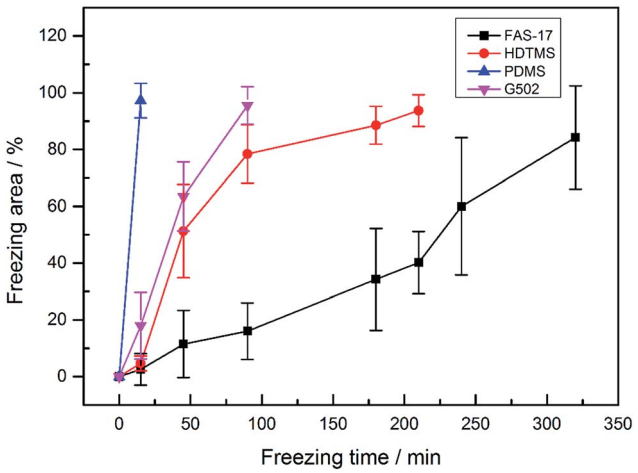

Fig. 6 Frosting area of the as-prepared SHP ZnO surfaces modified with FAS-17, G502, HDTMS, and PDMS.

coalescence of nearby condensed microdroplets on the SHP-PDMS and SHP-G502 surfaces. There was no evident self-transfer phenomenon observed on these two SHP surfaces. Therefore, the condensed microdroplets stayed motionless. However, self-transfer phenomena were detected on the SHP-HDTMS and SHP-FAS surfaces. Nearby condensed microdroplets on the SHP-HDTMS surface merged together and subsequently departed from their original locations as identified by a color change of the coalesced microdroplets resulting from a distance variation between the jumping water droplets and the lense. Meanwhile, as the jumping water droplets rolled along the surface they would pick up tiny droplets, impacting on the surface and sweeping it clean and dry. A similar phenomenon was observed on the SHP-FAS surface. Coalesced microdroplets would jump off the surface or stay in another position on the SHP-FAS surface after several bounces.

To further investigate the self-transfer phenomenon on the SHP-FAS surface, high speed cameras with a frame rate of 1000 frames per second was used. As shown in Fig. 9, a tiny droplet jumped off the surface and subsequently merged with a nearby droplet inducing a second bounce. As shown in the ESI video S1,† continually jumping water droplets jump off and subsequently fall back on the SHP-FAS surface. The coalescence of condensed microdroplets and the subsequent self-transfer movement on SHP-HDTMS and SHP-FAS markedly alter the diameter range and location of the condensed microdroplets. As a rational inference, the growth and distribution status of the condensed microdroplets on these two SHP surfaces exerts a large effect on the anti-frosting performance.

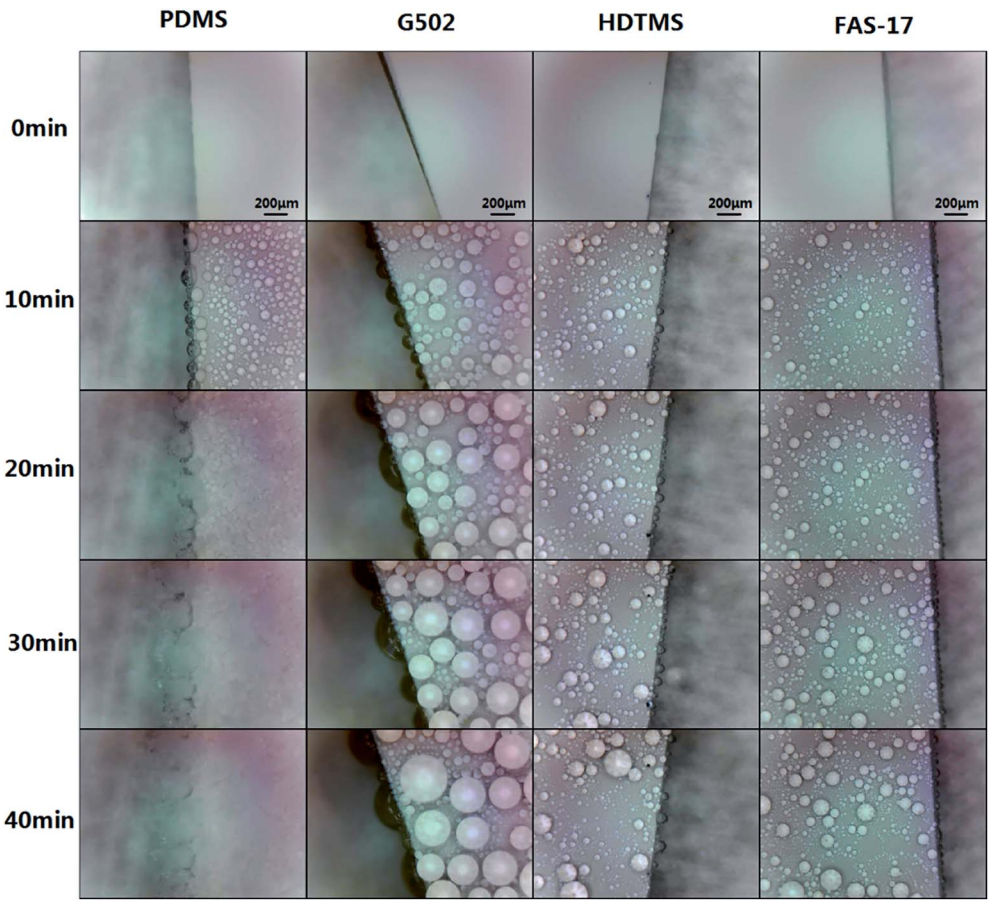

Fig. 7 Microscopic growth process of condensed water droplets on ZnO surfaces modified by PDMS, G502, HDTMS, and FAS-17.

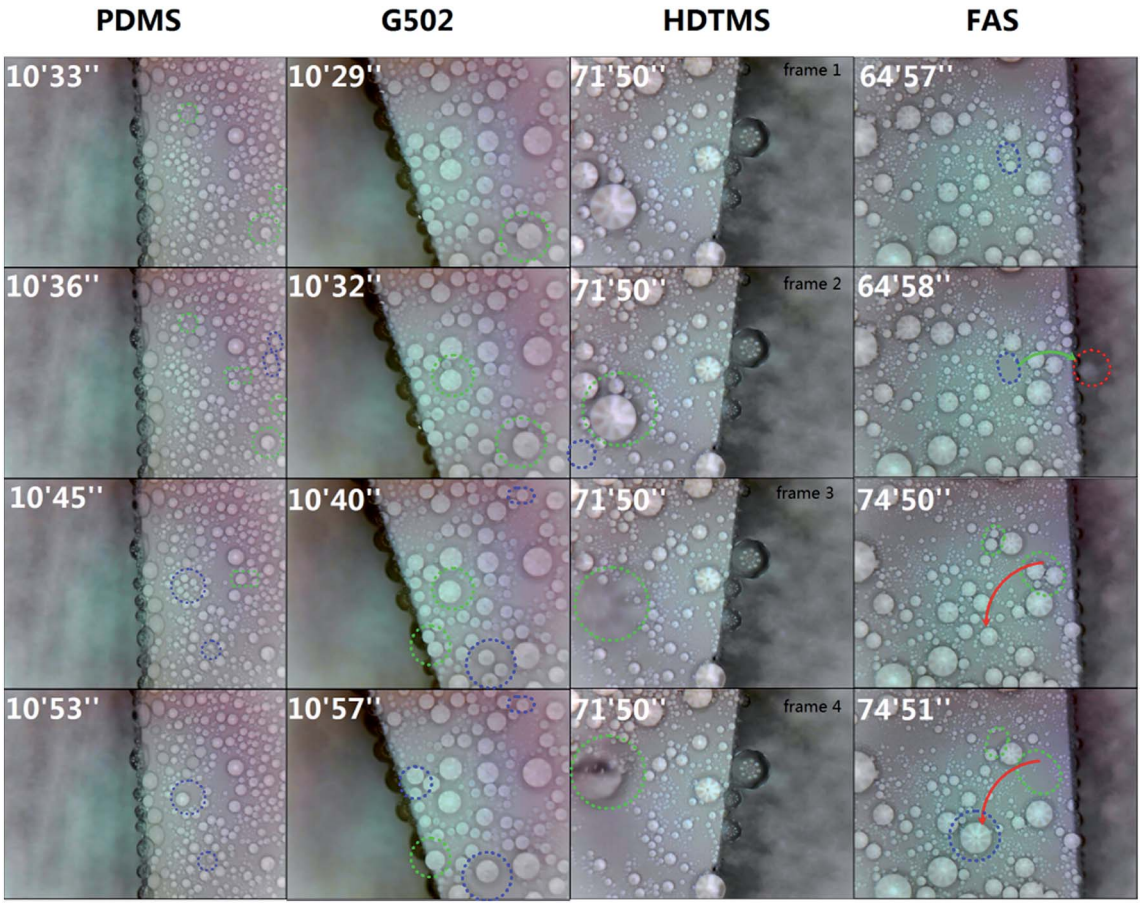

Fig. 8 Coalescence of condensed microdroplets on the PDMS, G502, HDTMS and FAS-17 modified SHP surfaces.

Due to the hydrophilic properties of the sample edges, frosting occurs first at these regions. Fig. S9† displays frost propagation on the four SHP surfaces which is illustrated in Fig. 10. The self-transfer movement on SHP-HDTMS and SHP-FAS demonstrates an obvious contrast to that on SHP-G502 and SHP-PDMS. The condensed water droplets freeze quickly on the SHP-PDMS surface indicating a faster heat transfer rate at low temperatures. The frozen water droplets behave like "defects" leading to a dramatically increased frost propagation rate. The "anchoring effect" on SHP-G502 and SHP-PDMS show that condensed water droplets grow in the "Wenzel state" on these two SHP surfaces leading to increased water volumes. According to $\Delta Q = Cm\Delta T$, it may take more time for the condensed water droplets (A and B) to freeze, which is why the frost on SHP-PDMS appears later than on SHP-HDTMS and SHP-FAS. However, the increased size of the condensed microdroplets minimizes the gap between the frozen droplets (C) and the nearby condensed microdroplets (A and B) making the frost crystals grow more easily across to the nearby condensed water droplets, which accelerates the frost propagation rate. Due to

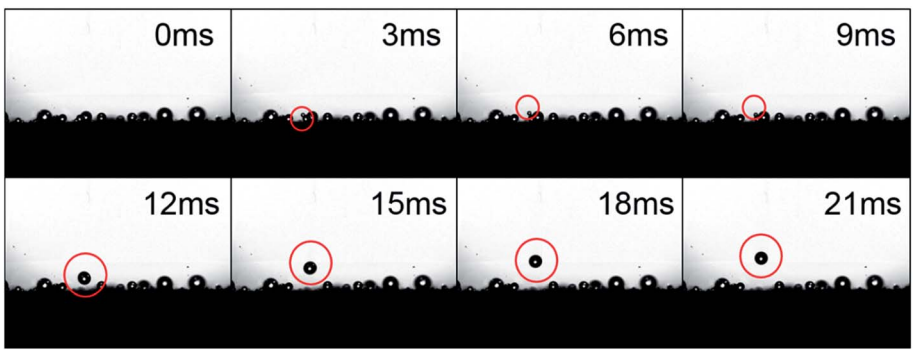

Fig. 9 Side view of the self-transfer phenomenon on FAS-17-modified SHP surfaces.

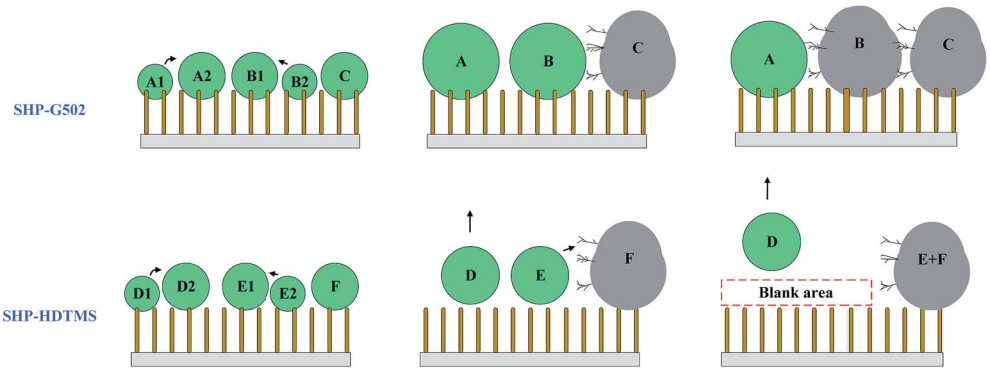

Fig. 10 Schematic of frost propagation on the SHP surfaces.

the self-transfer movement and the absorption of condensed water droplets by the frost front, a large "blank area" exists on SHP-HDTMS and SHP-FAS, which effectively inhibits the frosting propagation rate. This is the reason why the frost propagation rate on SHP-G502 is faster than that for SHP-HDTMS and SHP-FAS. According to the dimensionless form of Gibbs energy:[42]

$$G^* = F^{-2/3}(\theta)[2 - 2\cos\theta - \cos\theta_Y \sin^2\theta] \quad (1)$$

where $F(\theta) = (2 - 3\cos\theta + \cos^3\theta)$, θ is the intrinsic contact angle on a flat surface and θ_Y represents the contact angle on a rough surface. $\cos\theta_Y$ for droplets in the Cassie state and the Wenzel state can be described as $r\cos\theta$ and $f_s(1 + \cos\theta) - 1$, respectively. f_s is the solid–liquid fraction. FAS-17 mainly contains $-CF_3$ groups with a surface free energy of 6.7 mJ mol^{-1} which is lower than that of $-CH_3$ in HDTMS or other surface modifiers, which can better improve the intrinsic contact angle. The θ values for the flat surface modified with G502, HDTMS, FAS-17, and PDMS were measured to be 94.2°, 101.9°, 109.7° and 93.3°, respectively. f_s can be calculated to be 4.1% according to the CA measurement at ambient temperature where water droplets are supposed to be in the Cassie state. Given that the surfaces have comparable roughness, we converted the ZnO nanostructures into cylindrical structures referring to the average diameter of ZnO nanostructures (82.4 nm), equivalent film thickness (7.5 μm), and f_s (4.1%) as shown in Fig. S10.† The surface roughness r can be roughly calculated as 16.39. By defining $\Delta G = G_{Cassie} - G_{Wenzel}$, we can calculate the ΔG values for SHP-G502, SHP-HDTMS, SHP-FAS, and SHP-PDMS to be 0.3244, −0.9540, −1.8615, and 0.5057, respectively. If ΔG is negative, water vapor is more likely to condense in the Cassie state. The ΔG values for SHP-G502 and SHP-PDMS are both positive indicating that water vapor is prone to condense in the Wenzel state which is in accordance with the phenomenon observed in Fig. 7. The ΔG values for SHP-HDTMS and SHP-FAS are negative indicating that the water vapor condenses in the Cassie state and thus demonstrates a greater mobility because of the self-transfer phenomenon.

The excellent anti-frosting performance of SHP-HDTMS and SHP-FAS-17 can be attributed to the self-transfer movement. On one hand, the jumping droplets minimize the number of water droplets distributed on the surface, which in turn serves to slow down frost propagation by requiring longer inter-droplet ice bridges and sometimes even resulting in failed bridges owing to sufficiently spaced droplets completely evaporating before the bridges can connect. On the other hand, condensed water droplets are easily absorbed by the frost front because of a low adhesion force between the condensed microdroplets and the chilled SHP surface (Fig. S9†), leaving a large gap between the frost front and the condensed microdroplets. Thus, frost propagation is effectively inhibited by delaying the ice-bridging process.[21,43] These results demonstrate that the anti-frosting performance of SHP surfaces with the same nano-scale textures is largely affected by the surface modifiers. The surface modifier affects the condensation mode and subsequently the frosting propagation rate. The self-transfer movement plays a vital role in enhancing the anti-frosting performance of nanostructured SHP surfaces. By improving the anti-frosting property with the selection of FAS-17, the SHP surface can maintain superhydrophobicity at low temperatures which enhances the anti-icing property in glaze ice.

4. Conclusion

We have studied the anti-icing and anti-frosting properties of four SHP surfaces with different chemical compositions but the same nano-scale structures. Results show that SHP-FAS demonstrates the optimal anti-icing/frosting property compared to the other three SHP surfaces. Only 44% of the SHP-FAS surface froze after spraying it for 60 min in glaze ice and the frosting time is effectively delayed by over 320 min at −5 °C. Investigating the dynamics of the condensed water droplets has shed light on the source of the varied anti-icing/frosting property, which is determined by the mode of condensation on the SHP surfaces which have been modified with various surface modifiers. As the ΔG values are both negative for SHP-FAS and SHP-HDTMS, water vapor is prone to condense in the Cassie state leading to a self-transfer movement. The self-transfer movement can help sweep the SHP surface free of condensed water droplets and also inhibit the ice-bridging rate, which contributes to an enhancement in the anti-icing/frosting properties of the SHP surfaces. We can conclude that the chemical

composition has a large impact on the anti-frosting/icing performance of the SHP surfaces, which can be greatly improved by choosing an optimum surface modifier.

Conflicts of interest

There are no conflicts to declare.

Acknowledgements

We gratefully acknowledge the financial support from the Fundamental Research Funds for the Central Universities (2018) and National Natural Science Foundation of P. R. China (project no. 51377177).

References

1 X. Zhihai, J. Zhidong, G. Zhicheng, W. Liming, Z. Robing, Z. Yuming and L. Yan, Anti-icing performance of RTV coating with different resistivity on insulators, in *Electrical Insulation and Dielectric Phenomena (CEIDP), 2010 Annual Report Conference*, 2010, pp. 1–4.

2 X. Jiang, L. Shu, W. Sima, S. Xie and Q. Hu, Chinese Transmission Lines' Icing Characteristics And Analysis of Severe Ice Accidents, in *The Fourteenth International Offshore and Polar Engineering Conference*, International Society of Offshore and Polar Engineers, 2004.

3 X. Jiang, B. Dong, Y. Chao, Z. Zhang, Q. Hu, J. Hu and L. Shu, Diameter correction coefficient of ice thickness on conductors at natural ice observation stations, *IET Gener., Transm. Distrib.*, 2014, **8**, 11–16.

4 W. Barthlott and C. Neinhuis, Purity of the sacred lotus, or escape from contamination in biological surfaces, *Planta*, 1997, **202**, 1–8.

5 K. Liu, Z. Li, W. Wang and L. Jiang, Facile creation of bio-inspired superhydrophobic Ce-based metallic glass surfaces, *Appl. Phys. Lett.*, 2011, **99**, 261905.

6 Y. Shen, J. Tao, H. Tao, S. Chen, L. Pan and T. Wang, Anti-icing Potential of Superhydrophobic Ti_6Al_4V Surfaces: Ice Nucleation and Growth, *Langmuir*, 2015, **31**, 10799–10806.

7 Q. Zhang, M. He, J. Chen, J. Wang, Y. Song and L. Jiang, Anti-icing surfaces based on enhanced self-propelled jumping of condensed water microdroplets, *Chem. Commun.*, 2013, **49**, 4516–4518.

8 L. Mishchenko, B. Hatton, V. Bahadur, J. A. Taylor, T. Krupenkin and J. Aizenberg, Design of ice-free nanostructured surfaces based on repulsion of impacting water droplets, *ACS Nano*, 2010, **4**, 7699–7707.

9 R. Menini and M. Farzaneh, Elaboration of Al_2O_3/PTFE icephobic coatings for protecting aluminum surfaces, *Surf. Coat. Technol.*, 2009, **203**, 1941–1946.

10 P. Kim, T.-S. Wong, J. Alvarenga, M. J. Kreder, W. E. Adorno-Martinez and J. Aizenberg, Liquid-infused nanostructured surfaces with extreme anti-ice and anti-frost performance, *ACS Nano*, 2012, **6**, 6569–6577.

11 X. Yin, Y. Zhang, D. Wang, Z. Liu, Y. Liu, X. Pei, B. Yu and F. Zhou, Integration of Self-Lubrication and Near-Infrared Photothermogenesis for Excellent Anti-Icing/Deicing Performance, *Adv. Funct. Mater.*, 2015, **25**, 4237–4245.

12 N. Vogel, R. A. Belisle, B. Hatton, T. S. Wong and J. Aizenberg, Transparency and damage tolerance of patternable omniphobic lubricated surfaces based on inverse colloidal monolayers, *Nat. Commun.*, 2013, **4**, 2167.

13 S. B. Subramanyam, K. Rykaczewski and K. K. Varanasi, Ice adhesion on lubricant-impregnated textured surfaces, *Langmuir*, 2013, **29**, 13414–13418.

14 Y. Huang, M. Hu, S. Yi, X. Liu, H. Li, C. Huang, Y. Luo and Y. Li, Preparation and characterization of silica/fluorinated acrylate copolymers hybrid films and the investigation of their icephobicity, *Thin Solid Films*, 2012, **520**, 5644–5651.

15 M. Ruan, W. Li, B. Wang, B. Deng, F. Ma and Z. Yu, Preparation and Anti-icing Behavior of Superhydrophobic Surfaces on Aluminum Alloy Substrates, *Langmuir*, 2013, **29**, 8482–8491.

16 S. Farhadi, M. Farzaneh and S. Kulinich, Anti-icing performance of superhydrophobic surfaces, *Appl. Surf. Sci.*, 2011, **257**, 6264–6269.

17 S. Kulinich, S. Farhadi, K. Nose and X. Du, Superhydrophobic surfaces: are they really ice-repellent?, *Langmuir*, 2010, **27**, 25–29.

18 K. K. Varanasi, T. Deng, J. D. Smith, M. Hsu and N. Bhate, Frost formation and ice adhesion on superhydrophobic surfaces, *Appl. Phys. Lett.*, 2010, **97**, 234102.

19 J. B. Boreyko, B. R. Srijanto, T. D. Nguyen, C. Vega, M. Fuentes-Cabrera and C. P. Collier, Dynamic defrosting on nanostructured superhydrophobic surfaces, *Langmuir*, 2013, **29**, 9516–9524.

20 X. Chen, R. Ma, H. Zhou, X. Zhou, L. Che, S. Yao and Z. Wang, Activating the microscale edge effect in a hierarchical surface for frosting suppression and defrosting promotion, *Sci. Rep.*, 2013, **3**, 2515.

21 J. B. Boreyko and C. P. Collier, Delayed frost growth on jumping-drop superhydrophobic surfaces, *ACS Nano*, 2013, **7**, 1618–1627.

22 M. Wen, L. Wang, M. Zhang, L. Jiang and Y. Zheng, Antifogging and Icing-Delay Properties of Composite Micro- and Nanostructured Surfaces, *ACS Appl. Mater. Interfaces*, 2014, **6**, 3963–3968.

23 P. Guo, M. Wen, L. Wang and Y. Zheng, Strong anti-ice ability of nanohairs over micro-ratchet structures, *Nanoscale*, 2014, **6**, 3917–3920.

24 F. Xia and L. Jiang, Bio-Inspired, Smart, Multiscale Interfacial Materials, *Adv. Mater.*, 2008, **20**, 2842–2858.

25 W. Xu, J. Song, J. Sun, Y. Lu and Z. Yu, Rapid fabrication of large-area, corrosion-resistant superhydrophobic Mg alloy surfaces, *ACS Appl. Mater. Interfaces*, 2011, **3**, 4404–4414.

26 L. Cao, A. K. Jones, V. K. Sikka, J. Wu and D. Gao, Anti-icing superhydrophobic coatings, *Langmuir*, 2009, **25**, 12444–12448.

27 R. Jafari, R. Menini and M. Farzaneh, Superhydrophobic and icephobic surfaces prepared by RF-sputtered polytetrafluoroethylene coatings, *Appl. Surf. Sci.*, 2010, **257**, 1540–1543.

28 L. Yin, Y. Wang, J. Ding, Q. Wang and Q. Chen, Water condensation on superhydrophobic aluminum surfaces with different low-surface-energy coatings, *Appl. Surf. Sci.*, 2012, **258**, 4063–4068.

29 Y. Wang, M. Li, T. Lv, Q. Wang, Q. Chen and J. Ding, Influence of different chemical modifications on the icephobic properties of superhydrophobic surfaces in a condensate environment, *J. Mater. Chem. A*, 2015, **3**, 4967–4975.

30 M. J. Kreder, J. Alvarenga, P. Kim and J. Aizenberg, Design of anti-icing surfaces: smooth, textured or slippery?, *Nat. Rev. Mater.*, 2016, **1**, 15003.

31 Y. Shen, G. Wang, J. Tao, C. Zhu, S. Liu, M. Jin, Y. Xie and Z. Chen, Anti-Icing Performance of Superhydrophobic Texture Surfaces Depending on Reference Environments, *Adv. Mater. Interfaces*, 2017, **4**, 1700836.

32 X. Jiang, S. Wang, Z. Zhang, S. Xie and Y. Wang, Study on AC flashover performance and discharge process of polluted and iced IEC standard suspension insulator string, *IEEE Trans. Power Deliv.*, 2007, **22**, 472–480.

33 X. Jiang, J. Ma, Z. Zhang and J. Hu, Effect of hydrophobicity coating on insulator icing and DC flashover performance of iced insulators, *IEEE Trans. Dielectr. Electr. Insul.*, 2010, **17**, 351–359.

34 R. Liao, Z. Zuo, C. Guo, A. Zhuang, Y. Yuan, X. Zhao and Y. Zhang, Ice accretion on superhydrophobic insulators under freezing condition, *Cold Reg. Sci. Technol.*, 2015, **112**, 87–94.

35 R. Liao, Z. Zuo, C. Guo, Y. Yuan and A. Zhuang, Fabrication of superhydrophobic surface on aluminum by continuous chemical etching and its anti-icing property, *Appl. Surf. Sci.*, 2014, **317**, 701–709.

36 X.-H. Xu, H.-S. Wu, C.-J. Zhang and Z.-H. Jin, Morphological properties of AlN piezoelectric thin films deposited by DC reactive magnetron sputtering, *Thin Solid Films*, 2001, **388**, 62–67.

37 I. Sayago, M. Aleixandre, L. Ares, M. Fernandez, J. Santos, J. Gutierrez and M. Horrillo, The effect of the oxygen concentration and the rf power on the zinc oxide films properties deposited by magnetron sputtering, *Appl. Surf. Sci.*, 2005, **245**, 273–280.

38 P. Kelly and R. Arnell, Magnetron sputtering: a review of recent developmentsand applications, *Vacuum*, 2000, **56**, 159–172.

39 R. Liao, Z. Zuo, C. Guo, A. Zhuang, X. Zhao and Y. Yuan, Anti-icing performance in glaze ice of nanostructured film prepared by RF magnetron sputtering, *Appl. Surf. Sci.*, 2015, **356**, 539–545.

40 A. Hozumi, K. Ushiyama, H. Sugimura and O. Takai, Fluoroalkylsilane monolayers formed by chemical vapor surface modification on hydroxylated oxide surfaces, *Langmuir*, 1999, **15**, 7600–7604.

41 L. Xu, Z. Cai, Y. Shen, L. Wang and Y. Ding, Facile preparation of superhydrophobic polyester surfaces with fluoropolymer/SiO_2 nanocomposites based on vinyl nanosilica hydrosols, *J. Appl. Polym. Sci.*, 2014, **131**(11), 40340.

42 A. Marmur, Wetting on hydrophobic rough surfaces: To be heterogeneous or not to be?, *Langmuir*, 2003, **19**, 8343–8348.

43 Q. Xu, J. Li, J. Tian, J. Zhu and X. Gao, Energy-Effective Frost-Free Coatings Based on Superhydrophobic Aligned Nanocones, *ACS Appl. Mater. Interfaces*, 2014, **6**, 8976–8980.